

# Electron Transport through Thin Organic Films in Metal–Insulator–Metal Junctions Based on Self-Assembled Monolayers

R. Erik Holmlin,<sup>†</sup> Rainer Haag,<sup>†</sup> Michael L. Chabinye,<sup>†</sup> Rustem F. Ismagilov,<sup>†</sup> Adam E. Cohen,<sup>†</sup> Andreas Terfort,<sup>†</sup> Maria Anita Rampi,<sup>\*,‡</sup> and George M. Whitesides<sup>\*,†</sup>

Contribution from the Department of Chemistry and Chemical Biology, Harvard University, 12 Oxford Street, Cambridge, Massachusetts 02138, and Dipartimento di Chimica, Centro di Fotochimica CNR, Università di Ferrara, 44100 Ferrara, Italy

Received November 22, 2000

**Abstract:** This paper describes an experimentally simple system for measuring rates of electron transport across organic thin films having a range of molecular structures. The system uses a metal–insulator–metal junction based on self-assembled monolayers (SAMs); it is particularly easy to assemble. The junction consists of a SAM supported on a silver film (Ag-SAM(1)) in contact with a second SAM supported on the surface of a drop of mercury (Hg-SAM(2))—that is, a Ag-SAM(1)SAM(2)-Hg junction. SAM(1) and SAM(2) can be derived from the same or different thiols. The current that flowed across junctions with SAMs of aliphatic thiols or aromatic thiols on Ag and a SAM of hexadecane thiol on Hg depended both on the molecular structure and on the thickness of the SAM on Ag: the current density at a bias of 0.5 V ranged from  $2 \times 10^{-10}$  A/cm<sup>2</sup> for HS(CH<sub>2</sub>)<sub>15</sub>CH<sub>3</sub> on Ag to  $1 \times 10^{-6}$  A/cm<sup>2</sup> for HS(CH<sub>2</sub>)<sub>7</sub>CH<sub>3</sub> on Ag, and from  $3 \times 10^{-6}$  A/cm<sup>2</sup> for HS(Ph)<sub>3</sub>H (Ph = 1,4-C<sub>6</sub>H<sub>4</sub>) on Ag to  $7 \times 10^{-4}$  A/cm<sup>2</sup> for HSPhH on Ag. The current density increased roughly linearly with the area of contact between SAM(1) and SAM(2), and it was not different between Ag films that were 100 or 200 nm thick. The current–voltage curves were symmetrical around  $V = 0$ . The current density decreased with increasing distance between the electrodes according to the relation  $I = I_0 e^{-\beta d_{\text{Ag,Hg}}}$ , where  $d_{\text{Ag,Hg}}$  is the distance between the electrodes, and  $\beta$  is the structure-dependent attenuation factor for the molecules making up SAM(1). At an applied potential of 0.5 V,  $\beta$  was  $0.87 \pm 0.1 \text{ \AA}^{-1}$  for alkanethiols,  $0.61 \pm 0.1 \text{ \AA}^{-1}$  for oligophenylene thiols, and  $0.67 \pm 0.1 \text{ \AA}^{-1}$  for benzylic derivatives of oligophenylene thiols. The values of  $\beta$  did not depend significantly on applied potential over the range of 0.1 to 1 V. These junctions provide a test bed with which to screen the intrinsic electrical properties of SAMs made up of molecules with different structures; information obtained using these junctions will be useful in correlating molecular structure and rates of electron transport.

## Introduction

This paper describes a versatile junction that offers experimentally simple access to rates of electron transport across a wide range of organic thin films (Figure 1). We intend to use this junction as a test bed with which to correlate rates of electron transport with molecular structure across self-assembled monolayers (SAMs) sandwiched between two metal electrodes.<sup>1</sup> The work described in this paper provides reference values of important parameters against which data obtained using more complex systems can be compared.

Understanding how electrons flow through organic matter is important in several areas: rationalizing electron transfer in biological molecules; fabricating microelectronic devices and sensors; developing molecular electronics; and interpreting data from scanning tunneling microscopy (STM). Electron transport has been studied using a range of different experimental approaches.

**D–B–A Assemblies. (a) Synthetic Model Systems.** The experimental approaches to these questions that are most familiar

to chemists are those that have examined the rates of electron transfer from a donor (D) to an acceptor (A) through a molecular bridge (B) in solution in so-called D–B–A assemblies.<sup>2–13</sup> Studies of electron transfer in D–B–A assemblies have provided a substantial body of information about the relation

(2) Fox, M. A. *Acc. Chem. Res.* **1999**, 32, 201–207.

(3) Paddon-Row: M. N. *Acc. Chem. Res.* **1994**, 27, 18–25.

(4) Closs, G. L.; Miller, J. R. *Science* **1988**, 240, 440–447.

(5) Bowler, B. E.; Raphael, A. L.; Gray, H. B. *Prog. Inorg. Chem.* **1990**, 38, 259–322.

(6) Fox, L. S.; Kozik, M.; Winkler, J. R.; Gray, H. B. *Science* **1990**, 247, 1069–1071.

(7) Wasielewski, M. R. *Chem. Rev.* **1992**, 92, 435–461.

(8) MacQueen, D. B.; Schanze, K. S. *J. Am. Chem. Soc.* **1991**, 113, 7470–7479.

(9) Verhoeven, J. W.; Kroon, J.; Paddon-Row, M. N.; Oliver, A. M. In *Photoconversion Processes For Energy and Chemicals*; Hall, D. O., Grassi, G., Eds.; Elsevier: Amsterdam, The Netherlands, 1989; p 100.

(10) Paulson, B.; Pramrod, K.; Eaton, P.; Closs, G.; Miller, J. R. *J. Phys. Chem.* **1993**, 97, 13042–13045.

(11) Davis, W. B.; Svec, W. A.; Ratner, M. A.; Wasielewski, M. R. *Nature* **1998**, 396, 60–63.

(12) Helms A.; Heiler D.; McLendon, G. *J. Am. Chem. Soc.* **1992**, 114, 6227–6238.

(13) Scandola, F.; Chiorboli, C.; Indelli M. T.; Rampi, M. A. Covalently Linked Systems Containing Metal Complexes. In *Electron Transfer in Chemistry*; Balzani, V., Ed.; Wiley-VCH: Weinheim, 2001; Vol. III, Chapter 2.2, p 337.

\* To whom correspondence should be addressed.

<sup>†</sup> Harvard University.

<sup>‡</sup> Università di Ferrara.

(1) Holmlin, R. E.; Haag, R.; Ismagilov, R.; Rampi, M. A.; Whitesides, G. M. Submitted for publication.

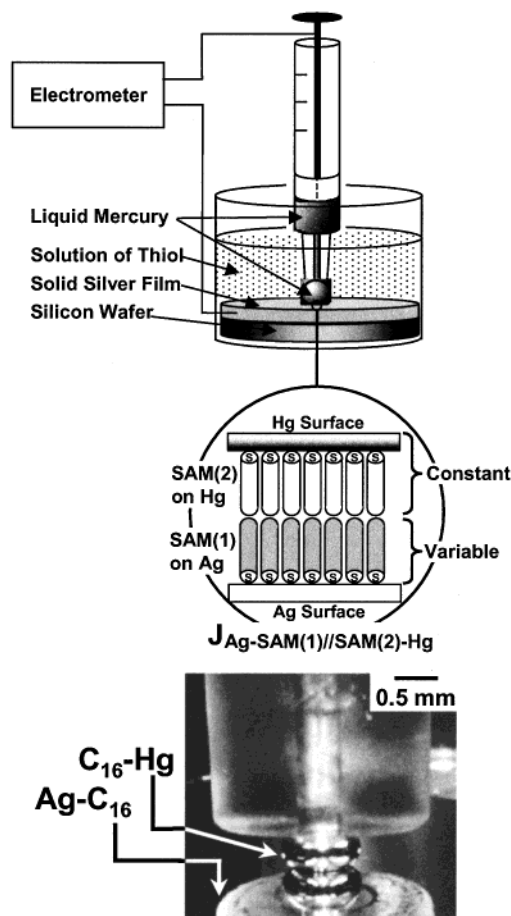


**Figure 1.** Schematic illustration of a  $J_{\text{Ag-SAM}(1)/\text{SAM}(2)\text{-Hg}}$  junction (the text explains the nomenclature). The photographic image is that of a  $J_{\text{Ag-C}_{16}/\text{C}_{16}\text{-Hg}}$  junction.

between rates of electron transfer and molecular structure. The extensive literature describing them<sup>2–12</sup> indicates that the rate of electron transfer ( $k_{\text{ET}}$ ) generally depends exponentially on distance according to eq 1 ( $k_0$  is a preexponential factor;  $\beta$  is a structure-dependent attenuation factor that describes the decay of electronic coupling between D and A as the distance separating them increases;  $d_{\text{D,A}}$  is the distance separating D and A).

$$k_{\text{ET}} = k_0 e^{-\beta d_{\text{D,A}}} \quad (1)$$

The value of the attenuation factor,  $\beta$ , depends significantly on the molecular structure of the bridge. Table 1 lists values of  $\beta$  that have been reported for D–B–A systems in which the bridge was composed of saturated hydrocarbons<sup>2–11</sup> and oligophenylenes.<sup>12</sup> These values are seldom accompanied by reliable estimates of uncertainty or of confidence limits, and it is currently difficult to judge when differences in  $\beta$  are significant. These values are all lower than the estimates of  $\beta$  (2.9–3.4  $\text{\AA}^{-1}$ ) based on a model of tunneling through vacuum assuming a rectangular barrier of height 5–10 eV.<sup>14,15</sup> The attenuation factor  $\beta$  has emerged as a characteristic parameter that can be used to classify the ability of molecular structures to provide a medium that facilitates tunneling from the D to the A, and to infer mechanistic details of the electron transfer. Despite the wide application of these systems, the organic

**Table 1.** Values of  $\beta$  for Organic Molecules Measured with Different Experimental Systems

system	composition of organics	$\beta$ ( $\text{\AA}^{-1}$ )	ref
D–B–A	saturated hydrocarbon	0.8–1.0	2–11
	oligophenylene	0.4–0.6	12
biological	photosynthetic reaction center	1.4	21, 22
	semisynthetic proteins	0.8–1.2	23
	DNA	0.1–1.4	28–33
electrochemical	alkanethiol SAM on Au	0.9–1.2	38–44
	oligo(phenyleneacetylene)	0.4–0.5	45, 46
MIM junction	SAM of Fatty acid on $\text{Al}/\text{Al}_2\text{O}_3$	1.5	48, 49
$J_{\text{Hg-SAM}/\text{SAM-Hg}}$ junction	alkanethiol SAM on Hg	0.8	60
CP-AFM	alkanethiol SAM on Au	1.1	75
STM	alkanethiol SAM on Au	1.2	109

synthesis that is required to obtain them can be difficult, and it is impractical to consider generating large sets of data using them. For this reason, they do not provide an ideally convenient strategy with which to study electron transfer across a range of molecular structures.

**(b) Biological Systems.** Electron transport has also been studied by a molecular approach in biological systems. Rates of electron transfer between different proteins of the photosynthetic reaction center have been measured by several groups.<sup>16–20</sup> Analysis of these rates by Dutton<sup>21,22</sup> yielded a value of  $\beta$  of 1.4  $\text{\AA}^{-1}$  for electron tunneling across proteins (Table 1). Gray<sup>23</sup> and others have studied electron transport in cytochromes, azurins, myoglobins, and iron–sulfur proteins.<sup>24–27</sup> Values of  $\beta$  in these systems have been reported to range from 0.8 to 1.2  $\text{\AA}^{-1}$  (Table 1).<sup>23</sup> These observations lead to the hypothesis that electron transfer in proteins takes place along well-defined pathways in different proteins. Electron transport across DNA has also been measured, and values of  $\beta$  for DNA have been reported to range from 0.1 to 1.4  $\text{\AA}^{-1}$  (Table 1).<sup>28–34</sup> These values now seem to represent transport by different mechanisms,

(16) Holten, D.; Windsor, W. W.; Thornber, J. P. *Biochem. Biophys. Acta* **1978**, *501*, 112–126.

(17) Gunner, M. R.; Dutton, P. L. *J. Am. Chem. Soc.* **1989**, *111*, 3400–3412.

(18) Schenck, C. C.; Blankenship, R. E.; Parson, W. W. *Biochem. Biophys. Acta* **1982**, *680*, 44–59.

(19) Chidsey, C. E. D.; Kirmaier, C.; Holten, D.; Boxer, S. G. *Biochem. Biophys. Acta* **1985**, *766*, 424–437.

(20) Takahashi, E.; Wraight, C. A. *FEBS Lett.* **1991**, *283*, 140–144.

(21) Page, C. C.; Moser, C. C.; Chen, X.; Dutton, P. L. *Nature* **1999**, *47*–52.

(22) Moser, C. C.; Keske, J. M.; Warncke, K.; Farid, R. S.; Dutton, P. L. *Nature* **1992**, *355*, 796–802.

(23) Winkler, J. R.; Di Bilio, A. J.; Farrow, N. A.; Richards, J. H.; Gray, H. B. *Pure Appl. Chem.* **1999**, *71*, 1753–1764.

(24) Wuttke, D. S.; Bjerrum, M. J.; Winkler, J. R.; Gray, H. B. *Science* **1992**, *256*, 1007–1009.

(25) Cowan, J. A.; Upmacis, R. K.; Beretan, D. N.; Onuchic, J. N.; Gray, H. B. *Ann. N.Y. Acad. Sci.* **1988**, *550*, 68–84.

(26) Mines, G. A.; Bjerum, M. J.; Hill, M. G.; Casimiro, D. R.; Chang, I.-J.; Winkler, J. R.; Gray, H. B. *J. Am. Chem. Soc.* **1996**, *118*, 1961–1965.

(27) Babini, E.; Bertini, I.; Borsari, M.; Capozzi, F.; Luchinat, C.; Zhang, X.; Moura, G. L. C.; Kurnikov, I. V.; Beratan, D. N.; Ponce, A.; Di Bilio, J. A.; Winkler, J. R.; Gray, H. B. *J. Am. Chem. Soc.* **2000**, *122*, 4532–4533.

(28) Kelley, S. O.; Barton, J. K. *Science* **1999**, *283*, 375–381.

(29) Lewis, F. D.; Wu, T. W.; Liu, X.; Letsinger, R. L.; Greenfield, S. R.; Miller, S. E.; Wasielewski, M. R. *J. Am. Chem. Soc.* **2000**, *122*, 2889–2902.

(30) Fukui, K.; Tanaka, K. *Angew. Chem., Int. Ed. Engl.* **1998**, *37*, 158–161.

(31) Wan, C.; Fiebig, T.; Kelley, S. O.; Treadway, C. R.; Barton, J. K.; Zewail, A. H. *Proc. Natl. Acad. Sci. U.S.A.* **1999**, *96*, 6014–6019.

(32) Harriman, A. *Angew. Chem., Int. Ed. Engl.* **1999**, *38*, 945–949.

(33) Meggers, E.; Michel-Beyerle, M. E.; Giese, B. *J. Am. Chem. Soc.* **1998**, *120*, 12950–12955.

(14) Gamow, G. Z. *Phys.* **1928**, *51*, 204–212.

(15) Onuchic, J. N.; Beratan, D. N.; Winkler, J. R.; Gray, H. B. *Annu. Rev. Biophys. Biomol. Struct.* **1992**, *21*, 349–377.

with the lowest values (i.e. the most conducting samples) dominated by hopping.<sup>28,29,34</sup> While the data describing electron transfer in biological systems are important for understanding tunneling in biology, the heterogeneity of the biological structures—and of the mechanisms of electron transport through them—makes interpretation of rates of electron transport in these systems difficult.

**Electrochemical Studies.** SAMs of organic thiols on the surface of metal electrodes (Ag, Au, and Hg) provide thin organic films with well-defined thicknesses that can be changed by varying the length of the organic groups.<sup>35–37</sup> Rates of electron transfer to a redox active molecule in solution above the SAM<sup>38–41</sup> or to one attached to the surface by a molecular tether<sup>42–47</sup> have been measured for films formed from a range of molecules with different structures. These rates also follow the relation in eq 1; values of  $\beta$  determined by this approach have been reported for alkanethiols<sup>38–44</sup> and for conjugated molecules derived from oligo(phenylacetylene) (Table 1).<sup>45,46</sup> The electrochemical approach is potentially limited by the range of rates of electron transfer that can be measured: measurements of high rates of electron transfer can require complicated experiments that are beyond the scope of the electrochemical technique.<sup>43</sup>

**MIM Junctions and SPM Systems.** Solid-state metal–insulator–metal (MIM) junctions, where electrons flow between metal surfaces that are separated by insulating films, have been used to study organic materials. Since the pioneering work of Mann and Kuhn,<sup>48</sup> several types of MIM junctions have been fabricated.<sup>49–54</sup> One of the challenges in fabricating these junctions is applying a second electrode onto a thin organic film adsorbed on a metal or semiconductor surface. This second electrode is frequently formed by evaporation of a metal onto

the surface of a Langmuir–Blodgett film or a SAM.<sup>48–54</sup> In this method of evaporation/condensation, metal atoms probably react with or damage the organic films, although these processes have not been characterized explicitly.

Reed<sup>55</sup> and Joachim<sup>56,57</sup> have used break junctions imaginatively in studying tunneling across benzenedithiols and oligothiophenes. Break junctions offer, in principle, the ability to characterize the conductance of single molecules and do not require the evaporation of a metal onto an organic layer, but they are difficult to characterize and they often fail due to electrical shorting.

To study organic thin films as nanoscale dielectrics, we developed a MIM junction that employs liquid Hg electrodes supporting SAMs of alkanethiols in van der Waals contact.<sup>1,58,59</sup> Majda used this junction to measure tunneling across SAMs sandwiched between the Hg electrodes.<sup>60</sup> He reported that the rate of electron transport across these junctions followed the relation described by eq 1, and determined a value of  $\beta = 0.8 \text{ \AA}^{-1}$  for SAMs of alkanethiols.

MIM junctions have also been developed using scanning probe microscopies (SPM) such as STM and atomic force microscopy (AFM). STM has been used as a junction where the tunneling electrons flow from the metal tip through an insulating layer to a metal surface on a solid substrate.<sup>61</sup> Several groups have used STM to probe tunneling across molecules in thin organic films<sup>62–71</sup> One of the difficulties in interpreting STM data is that the position of the probe and the conductivity of the sample are coupled, so it is difficult to establish the location of the tip relative to the sample. Conducting-probe AFM (CP-AFM) obviates this difficulty by controlling the position of a metal-coated tip with respect to the substrate using force feedback. This technique has been used to characterize electrical properties of a wide variety of organic systems.<sup>72–74</sup> In

(34) Henderson, P. T.; Jones, D.; Hampikian, G.; Kan, Y.; Schuster, G. B. *Proc. Natl. Acad. Sci. U.S.A.* **1999**, *96*, 8353–8358.

(35) Bain, C. D.; Troughton, E. B.; Tao, Y.-T.; Evall, J.; Whitesides, G. M.; Nuzzo, R. G. *J. Am. Chem. Soc.* **1989**, *111*, 321–335.

(36) Ulman, A. *An Introduction to Ultrathin Organic Films from Langmuir–Blodgett to Self-Assembly*; Academic Press: New York, 1991.

(37) Laibinis, P. E.; Palmer, B. J.; Lee, S. W.; Jennings, G. K. The synthesis of Organothiols and their Assembly in to Monolayers on Gold. In *Thin Solid Films*; Academic Press: Boston, MA, 1998; Vol. 24, pp 1–4.

(38) Finklea, H. O.; Hanshew, D. D. *J. Am. Chem. Soc.* **1992**, *114*, 3173–3181.

(39) Becka, A. M.; Miller, C. J. *J. Phys. Chem.* **1992**, *96*, 2657–2668.

(40) Miller, C.; Cuendet, P.; Grätzel, M. *J. Phys. Chem.* **1991**, *95*, 877–886.

(41) Slowinski, K.; Chamberlain, R. V.; Miller, C. J.; Majda, M. *J. Am. Chem. Soc.* **1997**, *119*, 11910–11919.

(42) Chidsey, C. E. D. *Science* **1991**, *251*, 919–922.

(43) Smalley, J. F.; Feldberg, S. W.; Chidsey, C. E. D.; Linford, M. R.; Newton, M. D.; Liu, Y. *J. Phys. Chem.* **1995**, *99*, 13141–13149.

(44) Weber, K.; Hockett, L.; Creager, S. *J. Phys. Chem. B* **1997**, *101*, 8286–8291.

(45) Creager, S.; Yu, C. Y.; Bamdad, C.; O'Connor, S.; MacLean, T.; Lam, E.; Chong, Y.; Olsen, G. T.; Luo, J.; Gozin, M.; Kayyem, J. F. *J. Am. Chem. Soc.* **1999**, *121*, 1056–1064.

(46) Sachs, S. B.; Dudeek, S. P.; Hsung, R. P.; Sita, L. R.; Smalley, J. F.; Newton, M. D.; Feldberg, S. W.; Chidsey, C. E. D. *J. Am. Chem. Soc.* **1997**, *119*, 10563–10564.

(47) Bakker, E. P. A. M.; Roest, A. L.; Marsman, A. W.; Jenneskens, L. W.; de Jong-van Steensel, L. I.; Kelly, J. J.; Vanmaekelbergh, D. *J. Phys. Chem. B* **2000**, *104*, 7266–7272.

(48) Mann, B.; Kuhn, H. *J. Appl. Phys.* **1971**, *42*, 4398–4405.

(49) Polymeropoulos, E. E. *J. Chem. Phys.* **1978**, *69*, 1836–1847.

(50) Metzger, R. M. *Acc. Chem. Res.* **1999**, *32*, 950–957.

(51) Collet, J.; Lenfant, S.; Vuillaume, D.; Bouloussa, O.; Rondelez, F.; Gay, J. M.; Kham, K.; Chevrot, C. *Appl. Phys. Lett.* **2000**, *76*, 1339–1341.

(52) Vuillaume, D.; Chen, B.; Metzger, M. *Langmuir* **1999**, *15*, 4011–4017.

(53) Boulas, C.; Collet, J.; Davidovits, J. V.; Rondelez, F. *Appl. Phys. Lett.* **1996**, *69*, 1646–1648.

(54) Zhou, C.; Despande, M. R.; Reed, M. A.; Jones, L., II; Tour, J. M. *Appl. Phys. Lett.* **1997**, *71*, 611–613.

(55) Reed, M. A.; Zhou, C.; Muller, C. J.; Burgin, T. P.; Tour, J. M. *Science* **1997**, *278*, 252–254.

(56) Magoga, M.; Joachim, C. *Phys. Rev. B* **1999**, *59*, 16011–16021.

(57) Kergueris, C.; Bourgoin, J. P.; Palacin, S.; Esteve, D.; Urbina, C.; Magoga, M.; Joachim, C. *Phys. Rev. B* **1999**, *59*, 12505–12513.

(58) Rampi, M. A.; Schueller, O. J.; Whitesides, G. M. *Appl. Phys. Lett.* **1998**, *72*, 1781–1783.

(59) Haag, R.; Rampi, M. A.; Holmlin, R. E.; Whitesides, G. M. *J. Am. Chem. Soc.* **1981**, *103*, 7895–7906.

(60) Slowinski, K.; Fong, H. K. Y.; Majda, M. *J. Am. Chem. Soc.* **1981**, *103*, 7257–7261.

(61) Weisendanger, R. *Scanning Probe Microscopy and Spectroscopy*; Cambridge University Press: Cambridge, 1994.

(62) Bumm, L. A.; Arnold, J. J.; Dunbar, T. D.; Allara, D. L.; Weiss, P. S. *J. Phys. Chem. B* **1999**, *103*, 8122–8127.

(63) Xue, Y.; Datta, S.; Hong, S.; Reifenberg, R.; Henderson, J. I.; Kubiak, C. P. *Phys. Rev. B* **1999**, *59*, R7852–R7855.

(64) Cygan, M. T.; Dunbar, T. D.; Arnold, J. J.; Bumm, L. A.; Shedlock, N. F.; Burgin, T. P.; Jones, L., II; Allara, D. L.; Tour, J. M.; Weiss, P. S. *J. Am. Chem. Soc.* **1998**, *120*, 2721–2732.

(65) Tian, W.; Datta, S.; Hong, S.; Reifenberg, R.; Henderson, J.; Kubiak, C. P. *J. Chem. Phys.* **1998**, *109*, 2874–2882.

(66) Zhou, S.; Liu, Y.; Xu, Y.; Hu, Z.; Qiu, X.; Wang, C.; Bai, C. *Chem. Phys. Lett.* **1998**, *297*, 77–82.

(67) Dhirani, A.-A.; Lin, P. H.; Guyot-Sionnest, P.; Zehner, R. W.; Sita, L. R. *J. Chem. Phys.* **1997**, *106*, 5249–5253.

(68) Datta, S.; Tian, W.; Hong, S.; Reifenberg, R.; Henderson, J. I.; Kubiak, C. P. *Phys. Rev. Lett.* **1997**, *79*, 2530–2533.

(69) Bumm, L. A.; Arnold, J. J.; Cygan, M. T.; Dunbar, T. D.; Burgin, T. P.; Jones, L.; Allara, D. L.; Tour, J. M.; Weiss, P. S. *Science* **1996**, *271*, 1705–1707.

(70) Joachim, C.; Gimzewski, J. K.; Schlitter, R. R.; Chavy, C. *Phys. Rev. Lett.* **1995**, *74*, 2102–2105.

(71) Langlais, V. J.; Schittler, R. R.; Tang, H.; Gourdon, A.; Joachim, C.; Gimzewski, J. K. *Phys. Rev. Lett.* **2000**, *83*, 2809–2812.

(72) Dai, H.; Wong, E. W.; Lieber, C. M. *Science* **1996**, *272*, 523–526.

(73) Yano, K.; Kyogaku, M.; Kuroda, R.; Shimada, Y.; Shido, S.; Matsuda, H.; Takimoto, K.; Albrecht, O.; Eguchi, K.; Nakagiri, T. *Appl. Phys. Lett.* **1996**, *68*, 188–190.

(74) Klein, D.; McEuen, P. *Appl. Phys. Lett.* **1995**, *66*, 2478–2480.

particular, Frisbie measured  $I$ - $V$  curves for SAMs of alkanethiols on Au.<sup>75</sup> Values of  $\beta$  measured by CP-AFM and STM (Table 1) are in agreement with those measured with molecular systems.

**Theory.** In the theory describing nonadiabatic electron transfer in molecular systems, the rate of electron transfer ( $k_{\text{ET}}$ ) is given by eq 2,<sup>76–80</sup> which explicitly separates contributions

$$k_{\text{ET}} = (4\pi/h)H_{\text{DA}}^2 (\text{FCWD}) \quad (2)$$

from the electronic and nuclear wave functions;  $H_{\text{DA}}$  describes the electronic coupling between the electronic wave functions of the donor (D) and the acceptor (A), and FCWD is the Franck–Condon weighted density of states that describes the overlap of nuclear wave functions of the reactant and the product.<sup>81</sup>  $H_{\text{DA}}$  (and therefore  $k_{\text{ET}}$ ) depends exponentially on the distance separating the electron donor and the electron acceptor because of the exponential drop-off of the electronic wave functions with distance (eq 3). A variety of strategies have

$$k_{\text{ET}} \propto H_{\text{DA}}^2 \propto \exp(-\beta d) \quad (3)$$

been employed to calculate  $H_{\text{DA}}$  for D–B–A assemblies.<sup>82–91</sup> Many of these approaches build on the superexchange model used by McConnell,<sup>92</sup> which assumes that indirect coupling between D and A takes place by mixing between electronic states on D and A and high-energy states on the bridging group (often called “virtual states”).

For electron transport between metal electrodes, the nuclear wave functions of the “reactant” and the “product” can be assumed to be identical and therefore the theoretical descriptions consider only the electronic wave functions. Mann and Kuhn<sup>48</sup> and Polymeropolous<sup>49</sup> used models for tunneling across a rectangular barrier to interpret electron transport across organic thin films in early MIM junctions.<sup>93,94</sup> In this model, the tunneling barrier is considered to be an unstructured barrier; the molecular structure of the medium is not considered. To our knowledge, this example is the only one where the abstract model of the rectangular barrier fits the experimental data.

(75) Wold, D. J.; Frisbie, C. D. *J. Am. Chem. Soc.* **2000**, *122*, 2970–2971.

(76) Marcus, R. A.; Sutin, N. *Biochim. Biophys. Acta* **1985**, *811*, 265–322.

(77) Barbara, P. F.; Meyer, T. J.; Ratner, M. A. *J. Phys. Chem.* **1996**, *100*, 13148–13168.

(78) Hush, N. S. *Coord. Chem. Rev.* **1985**, *64*, 135–157.

(79) Newton, M. D. *Chem. Rev.* **1991**, *91*, 767–792.

(80) Devault, D. *Quantum Mechanical Tunneling in Biological Systems*; Cambridge University Press: Cambridge, 1981.

(81) Methods for calculating FCWD have also been described: (a) Marcus, R. A. *J. Chem. Phys.* **1956**, *24*, 966–978. (b) Jortner, J. J. *J. Chem. Phys.* **1976**, *64*, 4860–4867. (c) Hopfield, J. J. *Proc. Natl. Acad. Sci. U.S.A.* **1974**, *71*, 3640–3644.

(82) Liang, C.; Newton, M. D. *J. Phys. Chem.* **1992**, *96*, 2855–2866.

(83) Liang, C.; Newton, M. D. *J. Phys. Chem.* **1993**, *97*, 3199–3211.

(84) Naleway, C. A.; Curtiss, L. A.; Miller, J. R. *J. Phys. Chem.* **1991**, *95*, 8434–8437.

(85) Beratan, D. N.; Hopfield, J. J. *J. Am. Chem. Soc.* **1984**, *106*, 1584–1594.

(86) Ratner, M. A. *J. Phys. Chem.* **1990**, *94*, 4877–4883.

(87) Reimers, J. R.; Hush, N. S. *Chem. Phys.* **1990**, *146*, 89–103.

(88) Siddarth, P.; Marcus, R. A. *J. Phys. Chem.* **1993**, *97*, 13078–13082.

(89) Evenson, J. W.; Karplus, M. *Science* **1993**, *262*, 1247–1249.

(90) Skourtis, S. S.; Regan, J. J.; Onuchic, J. N. *J. Phys. Chem.* **1994**, *98*, 3379–3388.

(91) *Advances in Chemical Physics, Volume 106, Electron Transfer—From Isolated Molecules to Biomolecules, Part One*; Jortner, J., Bixon, M., Eds.; John Wiley & Sons: New York, 1999.

(92) McConnell, H. M. *J. Chem. Phys.* **1961**, *35*, 508–515.

(93) Simmons, J. G. *J. Appl. Phys.* **1963**, *34*, 1793–1803.

(94) Hartman, T. E. *J. Appl. Phys.* **1964**, *35*, 3283–3294.

Electron transport through a tunneling barrier can exhibit a range of behaviors, depending on the size, the shape, the thickness of the barrier, and the character and density of defects.<sup>95</sup> The most prevalent behaviors are thermionic emission, direct tunneling, resonant tunneling, and hopping transport mediated by defects.<sup>96</sup>

More recently,<sup>97–100</sup> Bardeen’s<sup>101</sup> analysis of tunneling and Landauer’s<sup>102</sup> scattering formalism have been used to develop models for electron transport across molecules in MIM junctions. This approach relates the conductance ( $g$ ) to a transmission function,  $T$  (eq 4).<sup>97</sup>  $T$  is given by eq 5, where  $L$  is the length

$$g \propto (e^2/h)T^2 \quad (4)$$

$$T \sim e^{-2(mE_g)^{1/2}L/h} \quad (5)$$

of the molecule,  $E_g$  is the HOMO-LUMO gap,  $m$  is the rest mass of an electron, and  $h$  is Planck’s constant. It is interesting to observe the analogy between the transmission function  $T$  in eq 5 and the electronic coupling factor  $H_{\text{AB}}$  in eq 2; both  $H_{\text{AB}}$  and  $T$  depend exponentially on the length of the molecule.<sup>103</sup> As with calculations of  $H_{\text{DA}}$ , different methods have been used to calculate  $T$ .<sup>61,97,104</sup> The fitting of the  $I$ - $V$  experimental data in STM or MIM junctions with these models is still an issue under debate; the most difficult problem is how to treat the interaction between the molecules and the metal surfaces.<sup>105</sup>

**Experimental Design.** We agree with many of the others who have studied mechanisms of electron transfer through organic matter that a fruitful experimental approach to understanding them is to correlate rates of electron transfer with molecular structure, and to infer mechanism from these correlations. Our goal in this work is to develop an experimental system that can efficiently screen the electrical properties of a range of organic molecules with different structures. The system we use consists of a drop of Hg, supporting an alkanethiol SAM, in contact with the surface of another SAM supported by a second metal (Ag, Au, Cu, Hg).<sup>1,58,59</sup> The essential feature of these junctions is the SAM-coated Hg electrode. SAMs of organic thiols form easily on the surface of Hg with the thiols oriented perpendicularly to the metal surface. A liquid Hg surface supporting a SAM is compliant, and conforms to the topography of a solid surface with which it is brought in contact; this ability to conform minimizes the potential of shorting and of mechanical damage to the SAM, and also minimizes the influence of the nanometer-scale roughness of a SAM on a solid metal surface on rates of electron transport. The second electrode also contributes to the flexibility of the junction. We have assembled junctions both with liquid Hg as the second electrode and with a thin solid evaporated metal film (Ag, Au, Cu) as the second electrode; the latter were easier to assemble and manipulate than the former and had significantly fewer failures

(95) Barraud, A.; Millie, P.; Yakimenko, I. *J. Chem. Phys.* **1996**, *105*, 6972–6978.

(96) Chen, J.; Calvet, L. C.; Reed, M. A.; Carr, D. W.; Grubisha, D. S.; Bennett, D. W. *Chem. Phys. Lett.* **1999**, *313*, 741–788.

(97) Ratner, M. A.; Davis, B.; Kemp, M.; Mujica, V.; Roitberg, A.; Yaliraki, S. *Ann. N.Y. Acad. Sci.* **1998**, *852*, 22–37.

(98) Datta, S. *Electronic Transport in Mesoscopic Systems*; Cambridge University Press: Cambridge, 1995.

(99) Emberly, E. G.; Kirczenov, G. *Phys. Rev. B* **2000**, *61*, 5740.

(100) Mujica, V.; Roitberg, A. E.; Ratner, M. *J. Chem. Phys.* **2000**, *112*, 6934–6839.

(101) Bardeen, J. *Phys. Today* **1969**, *22*, 40–46 and references therein.

(102) Landauer, R. *Phys. Lett. A* **1981**, *8*, 91 and references therein.

(103) Segal, D.; Nitzan, A.; Ratner, M.; Davis, W. B. *J. Phys. Chem.* **2000**, *104*, 2790–2793.

(104) Magoga, M.; Joachim, C. *Phys. Rev. B* **1997**, *4722*–4729.

(105) Yaliraki, S. N.; Kemp, M.; Ratner, M. A. *J. Am. Chem. Soc.* **1999**, *121*, 3428–3434.

due to electrical and mechanical breakdown.<sup>58,60</sup> In addition, a system that uses one macroscopic, planar, solid electrode surface allows several consecutive measurements to be made on the same sample. We have concentrated on junctions that are formed from a Hg electrode supporting a single common alkanethiol SAM ( $\text{CH}_3(\text{CH}_2)_{14}\text{CH}_2\text{SH}$ ) and silver electrodes supporting a number of SAMs derived from different organic thiols (Figure 1).<sup>106</sup> We have assembled the junctions in hexadecane because it is insulating and minimizes background currents due to defects in the SAMs; solvents such as water and ethanol gave high background currents.

**Nomenclature.** To describe these junctions, we use the nomenclature  $J_{\text{Ag-SAM}(1)//\text{SAM}(2)\text{-Hg}}$ , where J indicates a junction, // represents van der Waals interactions at the interface between the terminal groups of the SAMs (typically  $-\text{X}/\text{H}_3\text{C}(\text{CH}_2)_n-$ ), SAM(1) indicates the SAM on the solid Ag electrode, and SAM(2) indicates the SAM on the Hg electrode. We refer to SAMs composed of alkanethiols,  $\text{HS}(\text{CH}_2)_{n-1}\text{CH}_3$  ( $n = 8, 10, 12, 14, 16$ ), by the notation  $\text{C}_n$ ; to aromatic SAMs composed of oligophenylene derivatives,  $\text{HS}(\text{C}_6\text{H}_4)_k-1\text{C}_6\text{H}_5$  ( $k = 1, 2, 3$ ) by the notation  $(\text{Ph})_k\text{H}$ ; and to aromatic SAMs composed of benzylic homologues of the oligophenylene thiols,  $\text{HSCH}_2(\text{C}_6\text{H}_4)_{m-1}\text{C}_6\text{H}_5$  ( $m = 1, 2, 3$ ), by the notation  $\text{CH}_2(\text{Ph})_m\text{H}$ .

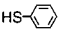
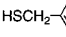
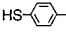
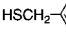
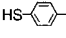
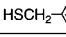
## Results and Discussion

**Fabrication and Electrical Stability of Junctions with Structure  $J_{\text{Ag-SAM}(1)//\text{SAM}(2)\text{-Hg}}$ .** (a) **Fabrication.** Figure 1 shows a schematic drawing of a typical  $J_{\text{Ag-SAM}(1)//\text{SAM}(2)\text{-Hg}}$  junction and a photographic image of a  $J_{\text{Ag-C}_{16}/\text{C}_{16}\text{-Hg}}$  junction. To assemble the junction, we formed a SAM on the surface of a thin evaporated film of silver by exposing it to a solution of the appropriate thiol in ethanol or THF (2 mM, 24–48 h). We then placed this electrode in a beaker and covered it with a solution of hexadecane containing  $\sim 1$  mM hexadecanethiol (HDT;  $\text{C}_{16}$ ). To form the SAM on the drop of Hg, we expressed a small drop ( $\sim 5 \mu\text{L}$ ) into a solution of HDT from a capillary connected to a reservoir of mercury; we allowed a SAM of HDT to form on the Hg surface for  $\sim 10$  min. A micromanipulator was then used to bring the HDT-covered mercury drop ( $\text{C}_{16}\text{-Hg}$ ) gently into contact with the SAM on the solid electrode. The area of interfacial contact was estimated using a microscope to magnify the image of the interface on a video monitor where its diameter could be measured and compared to the known diameter of the capillary that supported the drop. We applied a potential across the junction and recorded the current using an electrometer as both the voltage source and ammeter.

(b) **Electrical Breakdown of  $J_{\text{Ag-SAM}(1)//\text{SAM}(2)\text{-Hg}}$  Junctions.** The maximum voltage sustained by  $J_{\text{Ag-SAM}(1)//\text{SAM}(2)\text{-Hg}}$  junctions—the breakdown voltage (BDV)—sets the practical limit of the voltage range over which we can examine current flowing across the junctions. The BDV is revealed by an abrupt increase in current flowing across the junction in response to increasing applied potential; this electrical response is usually followed by irreversible mechanical breakdown in which the mercury forms an amalgam with the silver. Table 2 lists the values of the BDV, and the values of the electrical field at breakdown (BD-field) for the  $J_{\text{Ag-SAM}(1)//\text{SAM}(2)\text{-Hg}}$  junctions that we have examined in previous studies of the BDV,<sup>59</sup> and in this work. With the exception of  $J_{\text{Ag-(Ph)H}/\text{C}_{16}\text{-Hg}}$  and  $J_{\text{Ag-CH}_2(\text{Ph})\text{H}/\text{C}_{16}\text{-Hg}}$ , the junctions were stable to applied potentials above 1 V.

(106) We chose silver as the solid support because the molecules in both aliphatic and aromatic SAMs are known to have a smaller tilt angle with respect to the surface normal than that on a gold surface.<sup>120–122</sup>

**Table 2.** Summary of the Composition, Distance from Ag to Hg ( $d_{\text{M,Hg}}$ ), Current Density at 0.5 V, Breakdown Voltage (BDV), and Breakdown Field (BD-Field) for  $J_{\text{Ag-SAM}(1)//\text{SAM}(2)\text{-Hg}}$  Junctions

Thiol used to form SAM(1) on Ag	Thiol used to form SAM(2) on Hg	$d_{\text{Ag,Hg}}$ (nm) <sup>a</sup>	Current Density ( $\text{A}/\text{cm}^2$ ) <sup>b</sup>	BDV (V)	BD-Field (GV/m)
$\text{HS}(\text{CH}_2)_{15}\text{CH}_3$	$\text{HS}(\text{CH}_2)_{15}\text{CH}_3$	$3.6 \pm 0.2$	$1 \times 10^{-6}$	$1.7 \pm 0.4$	$0.5 \pm 0.1$
$\text{HS}(\text{CH}_2)_9\text{CH}_3$		$3.9 \pm 0.2$	$4 \times 10^{-7}$	$1.8 \pm 0.1$	$0.46 \pm 0.05$
$\text{HS}(\text{CH}_2)_{11}\text{CH}_3$		$4.1 \pm 0.2$	$5 \times 10^{-8}$	$1.9 \pm 0.1$	$0.46 \pm 0.05$
$\text{HS}(\text{CH}_2)_{13}\text{CH}_3$		$4.4 \pm 0.2$	$4 \times 10^{-9}$	$2.0 \pm 0.2$	$0.45 \pm 0.07$
$\text{HS}(\text{CH}_2)_{15}\text{CH}_3$		$4.6 \pm 0.2$	$2 \times 10^{-10}$	$2.5 \pm 0.4$	$0.5 \pm 0.1$
$\text{HS}(\text{CH}_2)_9\text{CH}_3$	$\text{HS}(\text{CH}_2)_{13}\text{CH}_3$	$3.6 \pm 0.2$	$5 \times 10^{-6}$	$1.9 \pm 0.2$	$0.53 \pm 0.09$
$\text{HS}(\text{CH}_2)_{11}\text{CH}_3$	$\text{HS}(\text{CH}_2)_{11}\text{CH}_3$	$3.6 \pm 0.2$	$8 \times 10^{-6}$	$1.9 \pm 0.3$	$0.5 \pm 0.1$
$\text{HS}$ - 	$\text{HS}(\text{CH}_2)_{15}\text{CH}_3$	$3.2 \pm 0.2$	$7 \times 10^{-4}$	$0.7 \pm 0.2$	$0.22 \pm 0.08$
$\text{HSCH}_2$ - 		$3.3 \pm 0.2$	$2 \times 10^{-4}$	$0.7 \pm 0.1$	$0.21 \pm 0.05$
$\text{HS}$ - 		$3.7 \pm 0.2$	$8 \times 10^{-5}$	$1.4 \pm 0.4$	$0.4 \pm 0.1$
$\text{HSCH}_2$ - 		$3.7 \pm 0.2$	$6 \times 10^{-5}$	$1.5 \pm 0.1$	$0.41 \pm 0.05$
$\text{HS}$ - 		$4.1 \pm 0.2$	$3 \times 10^{-6}$	$2.0 \pm 0.2$	$0.49 \pm 0.08$
$\text{HSCH}_2$ - 		$4.2 \pm 0.2$	$5 \times 10^{-7}$	$1.7 \pm 0.1$	$0.40 \pm 0.05$

<sup>a</sup> The method of estimating  $d_{\text{Ag,Hg}}$  is described in the Experimental Section. <sup>b</sup> Current density measured with an applied potential of 0.5 V.

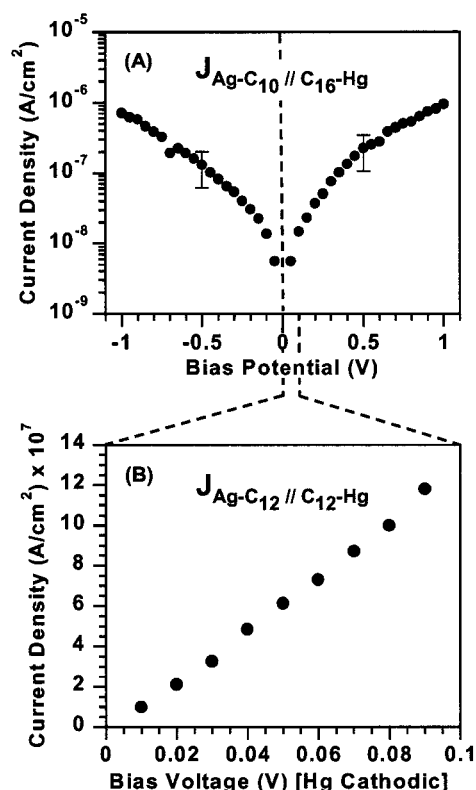


**Figure 2.** (A) Plot of current density (logarithmic scale) as a function of bias voltage over the range of  $-1$  to  $1$  V for a junction with structure  $J_{\text{Ag-C}_{10}/\text{C}_{16}\text{-Hg}}$ . The data are the average of four independent measurements with negative bias and four independent measurements with positive bias. The length of the error bars is representative of the standard deviation obtained from a statistically significant population of junctions (see section on reproducibility). (B) Plot of current density (linear scale) as a function of bias voltage over the range of  $0$ – $0.1$  V for a junction with structure  $J_{\text{Ag-C}_{12}/\text{C}_{12}\text{-Hg}}$ .

**Electron Transport across  $J_{\text{Ag-SAM}(1)//\text{SAM}(2)\text{-Hg}}$  Junctions.** (a)  **$I$ – $V$  Curves for  $J_{\text{Ag-SAM}(1)//\text{SAM}(2)\text{-Hg}}$  Junctions.** We measured the current that flowed across the junction in response to changes in potential ( $I$ – $V$  curve) over a range of  $0$ – $1$  V. Figure 2A shows an average of several  $I$ – $V$  curves for a junction with structure  $J_{\text{Ag-C}_{10}/\text{C}_{16}\text{-Hg}}$ . Figure 2B shows current density for  $J_{\text{Ag-C}_{12}/\text{C}_{12}\text{-Hg}}$  as a function of bias voltage from  $0$  to  $0.1$  V.

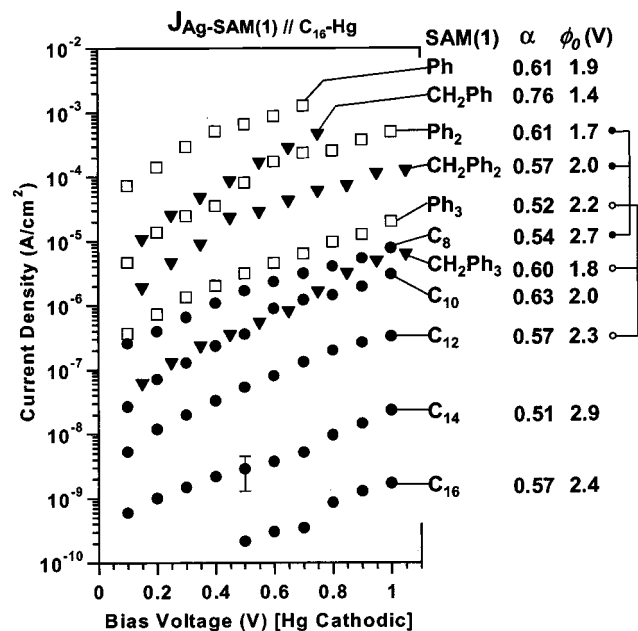


**Figure 3.** Plots of current density as a function of the bias voltage between the mercury and silver electrodes for  $J_{\text{Ag-SAM}(1)/\text{C}_{16}\text{-Hg}}$  junctions. The symbols used to represent different classes of compounds are the following: ●,  $\text{HS}(\text{CH}_2)_{n-1}\text{CH}_3$ ; □,  $\text{HS}(\text{Ph})_k\text{H}$  (all substitution of benzene rings is 1,4); and ◆,  $\text{HSCH}_2(\text{Ph})_m\text{H}$ . The length of the error bars is representative of the standard deviation obtained from a statistically significant population of junctions (see section on reproducibility). We list values of  $\phi_0$  (height of the tunneling barrier) and  $\alpha$  (an adjustable parameter that accounts for nonrectangular barriers) obtained by nonlinear least-squares fitting of the  $I$ - $V$  curve for each SAM on Ag to eq 9 (see section on data fitting). The lines connecting triads of data adjacent to the values of  $\phi_0$  and  $\alpha$  are for SAMs on Ag having the same thickness.

These plots show that the current density is nearly symmetric about  $V = 0$  V, and that it increases linearly at low bias potentials ( $V < 0.1$  V) and increases exponentially above  $\sim 0.1$  V. This combination of a linear relation to bias at low potentials and an exponential relation to bias at high potentials is consistent with tunneling of electrons across the junction.<sup>93-97,104</sup>

Figure 3 shows  $I$ - $V$  curves for  $J_{\text{Ag-SAM}(1)/\text{C}_{16}\text{-Hg}}$  junctions for SAMs of alkanethiols,  $\text{HS}(\text{CH}_2)_{n-1}\text{CH}_3$  ( $n = 8, 10, 12, 14, 16$ ), oligophenylene thiols,  $\text{HS}(\text{Ph})_k\text{H}$  ( $k = 1, 2, 3$ ), and benzylic homologues of the oligophenylene thiols,  $\text{HSCH}_2(\text{Ph})_m\text{H}$  ( $m = 1, 2, 3$ ). From these plots, we make three observations: (i) the shape of the  $I$ - $V$  curves is the same for  $\text{C}_n$ ,  $(\text{Ph})_k\text{H}$ , and  $\text{CH}_2$ - $(\text{Ph})_m\text{H}$ ; (ii) the current density measured for SAMs of the same thickness follows the order  $(\text{Ph})_k\text{H} > \text{CH}_2(\text{Ph})_m\text{H} > \text{C}_n$  (Table 2); and (iii) the magnitude of the current density depends on the thickness of the monolayers within a common series of compounds. Across this series of junctions, the current density changes over approximately 8 orders of magnitude. The ability to generate, easily and using the same experimental system, a series of junctions incorporating a range of structures and supporting a range of current densities is a strength of this system.

**(b) Parametric Sensitivities of Current Density.** We examined the sensitivity of the  $I$ - $V$  measurements to a variety of preparatory conditions. The details of these experiments are given in the Supporting Information. We outline the most important results of these studies in the following sections.

**(i) Location of the van der Waals Interface.** We sought to confirm that the  $I$ - $V$  curves for the different junctions did not depend on the physical location of the interface between SAM(1)

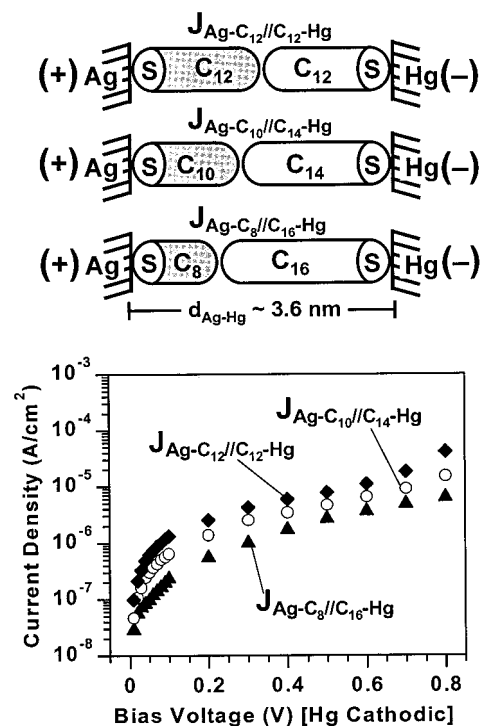


**Figure 4.** (A) Schematic illustration of three junctions in which the distance separating the electrodes was roughly the same for each junction ( $\sim 3.6$  nm) but the combination of thiols in SAM(1) and SAM(2) was different. (B) Plots of current density as a function of applied potential for the three  $J_{\text{Ag-SAM}(1)/\text{SAM}(2)\text{-Hg}}$  junctions pictured in part A. The symbols used to represent the different junctions are the following: ◆,  $J_{\text{Ag-C}_8/\text{C}_{16}\text{-Hg}}$ ; ○,  $J_{\text{Ag-C}_{10}/\text{C}_{14}\text{-Hg}}$ ; and ▲,  $J_{\text{Ag-C}_{12}/\text{C}_{12}\text{-Hg}}$ .

and SAM(2). We fabricated three junctions in which the distance between the electrodes ( $\sim 3.6$  nm) and the number of methylene groups separating them ( $\text{C}_{\text{tot}} = 24$ ) remained constant, but the interface between the SAMs was at a different position in each junction (Figure 4). Figure 4 shows the  $I$ - $V$  curves for the three junctions. Although the current density increases in the order  $J_{\text{Ag-C}_8/\text{C}_{16}\text{-Hg}} < J_{\text{Ag-C}_{10}/\text{C}_{14}\text{-Hg}} < J_{\text{Ag-C}_{12}/\text{C}_{12}\text{-Hg}}$ , the differences are small compared to the changes in current density for the series  $J_{\text{Ag-C}_n/\text{C}_{16}\text{-Hg}}$ , where  $n = 8, 10, 12$ . The close agreement between these  $I$ - $V$  curves supports the conclusion that the amount of current flowing across the junction depends on the thickness of the organic films sandwiched between the electrodes, and seems to be insensitive to the location of the interface between them.

**(ii) Roughness of the Silver Film.** The roughness of thin evaporated films of metal varies approximately as a constant fraction of the thickness of the film.<sup>107</sup> Although we expected Ag- $\text{C}_{10}$  SAMs supported on Ag that was 100 nm thick to be smoother than those on Ag that was 200 nm thick, the  $I$ - $V$  curves for the different junctions were not significantly different. This observation suggests that the surface of the SAM-coated Hg electrode is sufficiently compliant to conform to the surface of the SAM on Ag.

**(iii) Area of Contact.** For a given junction, the current density increased as the area of contact increased, although the relation between them was not perfectly linear. The scatter in the values of current density calculated for each area was representative of the experimental uncertainty that we observe for independent measurements of  $I$ - $V$  curves. To minimize errors associated with measurements of the area of contact, we used a micromanipulator to bring the two SAM-coated electrodes into contact,

(107) Ulman, A. *Chem. Rev.* 1996, 96, 1533-1554.

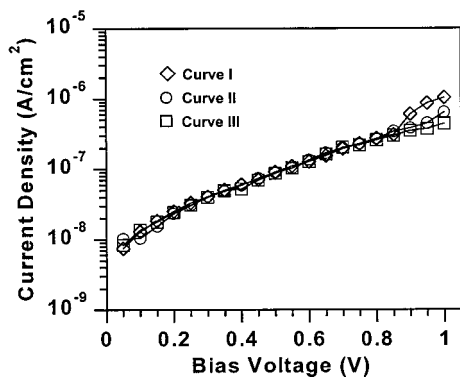


**Figure 5.** Plots of three  $I$ - $V$  curves obtained for a single junction with structure  $J_{\text{Ag-C}_{10}/\text{C}_{16}\text{-Hg}}$ . Each curve was recorded from 0 to 1 V. The junction broke down mechanically when the bias was applied to collect a fourth curve.

and used the same protocol for assembling each junction. The area of contact for all other junctions in this work ranged from  $1.5 \times 10^{-3}$  to  $3 \times 10^{-3}$   $\text{cm}^2$ ; this range showed the least amount of scatter.

**(iv) Solvent.** We assembled  $J_{\text{Ag-C}_{10}/\text{C}_{16}\text{-Hg}}$  junctions in a variety of different solvents and compared the current density across them to that observed with hexadecane as the solvent. The current density across junctions formed in hydrocarbon solvents of differing structure—isoctane, hexane, and toluene—was essentially indistinguishable from that across junctions formed in hexadecane. This observation suggests that the solvent does not disrupt the structure of the SAMs even if the solvent is intercalating in defect sites.

**(v) Purity of Thiol and Preparation of SAMs.** To form aliphatic SAMs, we use commercially available alkanethiols without purifying them. Because these thiols may contain disulfides, we tested SAMs formed from solutions of thiol with a known ratio of thiol to disulfide. The presence of the disulfide did not affect the current density.

**(c) Net Reproducibility.** We have established the reproducibility of four different aspects of these junctions: (i) the fraction of a group of junctions that are functional; (ii) the experimental uncertainty of  $I$ - $V$  curves obtained for a statistically significant number of independent junctions with identical configurations; (iii) the reproducibility of the  $I$ - $V$  curve obtained from a single junction; and (iv) the temporal stability of the current at a constant potential.

Out of a group of 30 independent  $J_{\text{Ag-C}_{10}/\text{C}_{16}\text{-Hg}}$  junctions formed from 30 different Hg-SAM electrodes and 6 different Ag-SAM electrodes (each Ag-SAM electrode had enough room to accommodate about five different contact areas), 21 of them were functional and yielded  $I$ - $V$  curves. Five of the junctions were mechanically stable but exhibited currents that were in the range of mA, suggesting that there was a short distance between the two electrodes. Four of the junctions broke down mechanically immediately after a voltage was applied. Therefore, 70% of the junctions in this group were functional. This fraction is substantially greater than that reported (24%) for junctions with upper electrodes that were fabricated by metal vapor deposition.<sup>52</sup>

The range from the lowest to highest value (at a particular bias voltage) of the current density measured across the 21 independent  $J_{\text{Ag-C}_{10}/\text{C}_{16}\text{-Hg}}$  junctions was approximately a factor of 10. The magnitude of the standard deviations from the average current density were approximately  $\pm 55\%$  of the average current density for each bias voltage. Figure 5 shows three  $I$ - $V$  curves that were measured for the same  $J_{\text{Ag-C}_{10}/\text{C}_{16}\text{-Hg}}$

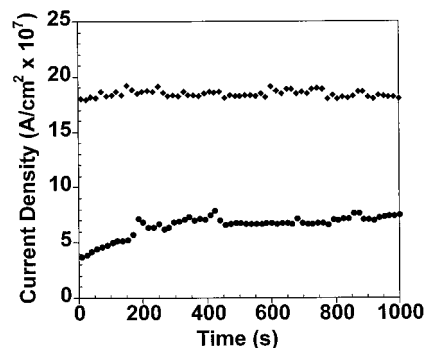


**Figure 6.** Plot of current as a function of time for a junction with the structure  $J_{\text{Ag-C}_{10}/\text{C}_{16}\text{-Hg}}$ . The first data set in the figure ( $\bullet$ ) was measured by increasing the bias on the junction from 0 to 0.5 V over 40 s. The second data set ( $\blacklozenge$ ) was taken using the same procedure on the same junction approximately 20 min later. During the 20 min period between these measurements the bias on the junction was held at 1 V (data not shown).

junction. The junction was assembled, and the first curve was recorded by increasing the voltage from 0 to 1 V. The bias was then returned to 0 V and another curve obtained by increasing the voltage to 1 V. This process was repeated to obtain the third curve. The junction failed mechanically when we attempted to collect a fourth curve. The figure shows that the magnitude of the current is effectively indistinguishable for the three curves. These observations suggest that the range in current density observed for different junctions with the same composition reflects variations in their composition. We believe that these variations are mostly due to uncertainties in the measured areas of contact.

We tested the temporal stability of a  $J_{\text{Ag-C}_{10}/\text{C}_{16}\text{-Hg}}$  junction by ramping the bias voltage to a setpoint and then holding the bias fixed for a period of time while measuring the current (Figure 6). We then repeated the process several times on the same junction. We tested three independent junctions to verify the reproducibility of the data. We observed that the current increases by less than a factor of 4 over time scales of hundreds of seconds during the first application of voltage. On subsequent constant voltage measurements, the current is more stable, but is larger than that observed during the first time measurement (less than a factor of 4 higher for the three separate junctions tested). These changes were small relative to the range of currents measured over a 1 V range for the junctions that we tested. These data differ from the work of Majda where a large current jump was observed over a similar time period in a Hg-SAM//SAM-Hg junction.<sup>108</sup> Our data show that the current measured in our junction is stable to repeated measurements over a period of at least 1 h.

**(d) Distance Dependence of Current Density in  $J_{\text{Ag-SAM}(1)/\text{C}_{16}\text{-Hg}}$  Junctions.** Using thiols with different lengths and molecular structures, we fabricated a series of junctions in which the distance separating the Ag and Hg electrodes varied systematically. Figure 7 plots the current density (bias = 0.5 V) on a logarithmic scale against the separation of the electrodes,  $d_{\text{Ag,Hg}}$ , for junctions with aliphatic SAMs on Ag and junctions with aromatic SAMs on Ag. We estimated  $d_{\text{Ag,Hg}}$  by adding the thicknesses of the SAM on Ag and of the SAM on Hg (see Experimental Section for details). For bias potentials over the range of 0.1 to 1 V, the current density decreased with increasing  $d_{\text{Ag,Hg}}$  according to the relation in eq 6. This observation of an exponential decrease in current with distance is consistent with

(108) Slowinski, K.; Majda, M. *J. Electroanal. Chem.* **2000**, 491, 139–147.

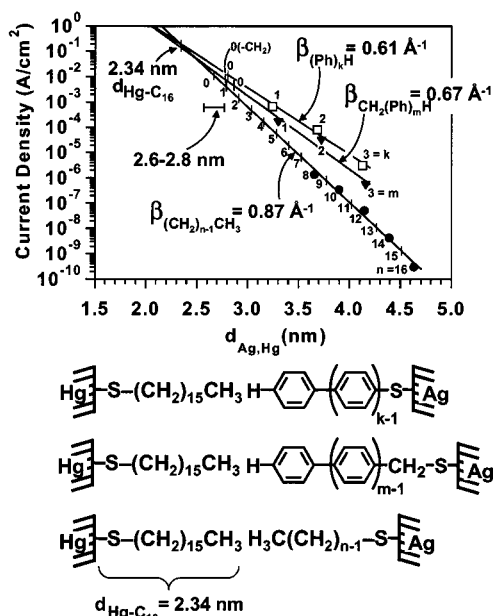


**Figure 7.** (A) Plot comparing the distance dependence of the current density in  $J_{\text{Ag-SAM}(1)/\text{C}_{16}\text{-Hg}}$  junctions for SAMs composed of aliphatic thiols ( $\text{HS}(\text{CH}_2)_{n-1}\text{CH}_3$ ; solid circles) and for SAMs composed of oligophenylene thiols ( $\text{HS}(\text{Ph})_k\text{H}$ ; open squares) and for their benzylic homologues ( $\text{HSCH}_2(\text{Ph})_m\text{H}$ ; solid triangles). Current densities were obtained at 0.5 V bias. The solid lines through the data points correspond to computer-generated, linear least squares fits of the natural log of current density to  $\ln(I) = -\beta d_{\text{Ag,Hg}} + \ln(I_0)$ . The error in  $\beta$  is  $\sim 0.1 \text{ \AA}^{-1}$ . (B) Schematic representation of junctions formed from the three classes of thiols.

a mechanism for electron transport in which the current flowing across the junction is due to tunneling.<sup>93–97,104</sup>

$$I = I_0 e^{-\beta d_{\text{Ag,Hg}}} \quad (6)$$

Since current in a tunneling junction is proportional to the probability of tunneling, the current flowing through  $J_{\text{Ag-SAM}(1)/\text{SAM}(2)\text{-Hg}}$  can be expressed as the product of the probability of tunneling through each SAM<sup>109</sup> separately. Thus, current density ( $I$ ) can be expressed with eq 7 where  $\beta(1)$  and  $\beta(2)$  are the attenuation factors characteristic of the molecules forming SAM(1) and SAM(2), and  $d_{\text{SAM}(1)}$  and  $d_{\text{SAM}(2)}$  are the thicknesses of the two SAMs. Because SAM(2) is a constant component of these junctions,  $e^{-\beta(2)d_{\text{SAM}(2)}}$  is a constant ( $\gamma$ ), so  $I$  is given by eq 8; this analysis assumes that any scattering at the interfaces between SAM(1) and SAM(2) is constant for SAM(1) formed from aliphatic thiols and SAM(1) formed from aromatic thiols. The slopes of the lines in Figure 6 therefore give the attenuation factor for the molecules forming SAM(1) on Ag.

$$I \cong I_0 [e^{-\beta(1)d_{\text{SAM}(1)}}] [e^{-\beta(2)d_{\text{SAM}(2)}}] \quad (7)$$

$$I \cong I_0 \gamma e^{-\beta(1)d_{\text{SAM}(1)}} \quad (8)$$

Figure 8 plots the values of  $\beta$  as a function of voltage for the three different SAMs on Ag. These values of  $\beta$  are in good agreement with corresponding values obtained by photoinduced electron transfer in molecular D–B–A systems<sup>2–12</sup> and by electron transfer between a solid electrode and redox-active species in solution (Table 1).<sup>38–44</sup> In work that can be compared

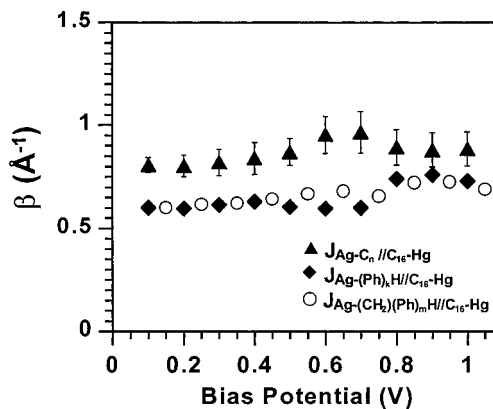


**Figure 8.** Plots of the attenuation factor  $\beta$  as a function of applied potential. The symbols are defined on the plot. The data for  $J_{\text{Ag-CH}_2(\text{Ph})_m\text{H}/\text{C}_{16}\text{-Hg}}$  were shifted on the x-axis by 50 mV for clarity of presentation. The error bars are those calculated with the least-squares fitting routine used to calculate  $\beta$ .

directly with that reported here, Majda found  $\beta = 0.8 \pm 0.1 \text{ \AA}^{-1}$  for alkanethiols in  $J_{\text{Hg-SAM}/\text{SAM-Hg}}$ .<sup>60</sup> The agreement among these several values of  $\beta$  suggests that the mechanism of charge transport in these solid-state junctions is closely related to the mechanism of electron transfer in soluble molecular systems, and between solid electrodes and soluble molecules in electrochemical systems.

The values of  $\beta$  for aromatic and aliphatic SAMs did not change significantly over the range of 0 to 1 V. Majda also found that values of  $\beta$  measured in  $J_{\text{Hg-SAM}/\text{SAM-Hg}}$  junctions did not change significantly over the same voltage range.<sup>60</sup> In an electrochemical system, Becka and Miller<sup>39</sup> reported that values of  $\beta$  for electron transport through aliphatic SAMs on Au changed by <10% over a range of overpotentials that differed by more than 1 V; they concluded that the tunneling barrier was effectively independent of voltage over this range.

Figure 7 also summarizes an analysis that establishes the internal consistency of the data for the three sets of junctions,  $J_{\text{Ag-S}(\text{CH}_2)_{n-1}\text{CH}_3/\text{C}_{16}\text{-Hg}}$ ,  $J_{\text{Ag-(Ph)}_k\text{H}/\text{C}_{16}\text{-Hg}}$ , and  $J_{\text{Ag-CH}_2(\text{Ph})_m\text{H}/\text{C}_{16}\text{-Hg}}$ . We extrapolated plots of current density against  $d_{\text{Ag,Hg}}$  for each of the three junctions to their intersection points. These points should, in principle, reflect values of  $d_{\text{Ag,Hg}}$  for hypothetical junctions with the same composition: (i) a junction with no contribution from an organic monolayer on silver, that is,  $J_{\text{Ag}/\text{C}_{16}\text{-Hg}}$  ( $d_{\text{Ag,Hg}} = 2.34 \text{ nm}$ ), or (ii) junctions in which the organic groups on silver had been removed, and only the Ag–S bond and the van der Waals radius of the terminal methyl group or hydrogen atom remained, that is,  $J_{\text{Ag-SH}/\text{C}_{16}\text{-Hg}}$  or  $J_{\text{Ag-SCH}_3/\text{C}_{16}\text{-Hg}}$  ( $d_{\text{Ag,Hg}} = 2.6\text{--}2.8 \text{ nm}$ ). The difference between 2.34 and 2.6–2.8 nm, 0.3–0.5 nm, is a reasonable value for an aggregate contribution to the thickness from the Ag–S bond, the S–C bond, and the van der Waals radii of the terminal groups. The intersection region in Figure 7 occurs comfortably within this region. The consistency of our data for the three sets of organic compounds suggests that they are giving directly comparable data.

(e) **Fitting  $I$ – $V$  Curves with a Modified Model for Tunneling through a Rectangular Barrier.** The determination of a detailed mechanism for electron transport is a difficult problem. In the absence of variable-temperature data, we do not have the information that is required to separate out many possible mechanisms. We would, however, like to have a model that would allow us to fit three of the characteristics of the tunneling currents we have measured: (i) the shape of the  $I$ – $V$  curve; (ii) the magnitude of the attenuation factor  $\beta$ ; and (iii)

(109) Weiss, P. S.; Bumm, L. A.; Dunbar, T. D.; Burgin, T. P.; Tour, J. M.; Allara, D. L. *Ann. N.Y. Acad. Sci.* **1998** 852, 145–177.



the voltage dependence of  $\beta$  over the range of 0.1–1 V. We started our analysis using the simplest physical model available, that is, a structureless, one-dimensional rectangular barrier. This model is expressed by eq 9 (taking  $\alpha = 1$ ).<sup>61,93,94</sup> We conclude that this model is *not* compatible with the data, but it is important to describe the evidence leading to that conclusion.

$$I = C_0 \frac{e}{4\pi^2 \hbar d^2} \left\{ \left( e\phi_0 - \frac{eV}{2} \right) \times \exp \left[ -\frac{2(2m)^{1/2}}{\hbar} \alpha \left( e\phi_0 - \frac{eV}{2} \right)^{1/2} d \right] - \left( e\phi_0 + \frac{eV}{2} \right) \times \exp \left[ -\frac{2(2m)^{1/2}}{\hbar} \alpha \left( e\phi_0 + \frac{eV}{2} \right)^{1/2} d \right] \right\} \quad (9)$$

$$\beta = \frac{2(2m)^{1/2}}{\hbar} \alpha \left( e\phi_0 - \frac{eV}{2} \right)^{1/2} \quad (10)$$

$$\phi_0 = \frac{\beta^2 \hbar^2}{8m\alpha^2 e} + \frac{V}{2} \quad (11)$$

This equation expresses current density  $I$  (in A/cm<sup>2</sup>) due to electron tunneling through a barrier of height  $\phi_0$  (in Volts) as a function of applied voltage  $V$  (in Volts;  $C_0$  is a unitless preexponential factor;  $m$  is the rest mass of an electron (in kg),  $\hbar$  is Planck's constant (in J s) divided by  $2\pi$ ,  $e$  is the charge of an electron (in Coulombs),  $\alpha$  is a unitless adjustable parameter used in fitting, and  $d$  is the tunneling distance (in m;  $d'$  is the tunneling distance in cm)). The assumptions underlying this model are the following: (i) the height of the barrier is constant over the entire tunneling distance, i.e. the barrier is rectangular; (ii) the dielectric constant of the medium composing the barrier is uniform and does not affect the shape of the barrier; (iii) the current density is independent of temperature; and (iv) the height and width of the barrier are independent of image potential. The exponential terms in eq 9 provide a relation between the attenuation factor  $\beta$ ,  $\phi_0$ , and  $V$  (eq 10). Solving eq 10 for  $\phi_0$  provides a relation from which to calculate  $\phi_0$  from observed values of  $\beta$  (eq 11). To determine whether this model was compatible with our results we compared several characteristics of these equations to experimental  $I$ – $V$  curves using the junction with structure J<sub>Ag–C<sub>10</sub>/C<sub>16</sub>–Hg</sub> and to values of  $\beta$  as a function of bias potential.

**(i) Estimating  $\phi_0$  from Experimental  $\beta$  and Calculated  $I$ – $V$  Curves with Equation 9 ( $\alpha = 1$ ).** Using eq 11 and the value of  $\beta = 0.83 \text{ \AA}^{-1}$  (at 0.1 V) we estimated the height of a hypothetical rectangular barrier to be  $\phi_0 = 0.67 \text{ V}$ . This barrier height is substantially lower than that expected if the Fermi level of the silver electrode lies halfway between the HOMO and LUMO of the aliphatic chain.<sup>110</sup> Using these derived parameters, neither the  $I$ – $V$  curve calculated using eq 10 (Figure 9) nor the voltage dependence of  $\beta$ <sup>111</sup> fit the experimental results.

**Nonlinear Least-Squares Fitting of Equation 9 ( $\alpha = 1$ ) to an Experimental  $I$ – $V$  Curve.** We have also used nonlinear least-squares fitting to fit eq 9 to the observed  $I$ – $V$  curve by allowing  $\phi_0$  and  $C_0$  to vary. This method fits the observed  $I$ – $V$  curve with  $\phi_0 = 5.3 \text{ V}$  (Figure 9), but produces a value of  $\beta$  ( $\sim 2.3 \text{ \AA}^{-1}$ ) that is substantially larger than that of the observed values ( $\sim 0.9 \text{ \AA}^{-1}$ ). For this reason, we do not believe that the derived value of the barrier height is reasonable.

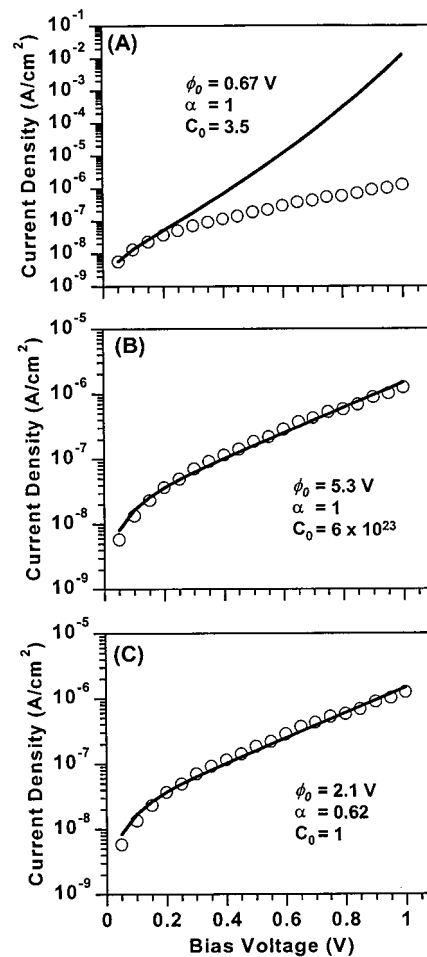


**Figure 9.** Plots comparing average current density observed for a junction with structure J<sub>Ag–C<sub>10</sub>/C<sub>16</sub>–Hg</sub> (open symbols) to current density calculated (solid lines) with eq 9 in the text; the parameters used in the calculation of the different curves are indicated on the plots. In part B the values of  $\phi_0$  and  $C_0$  and in part C the values of  $\phi_0$  and  $\alpha$  were obtained by nonlinear least-squares fitting of the 21 independent  $I$ – $V$  curves plotted in Figure 8A to eq 9.

Given the incompatibility of these calculations with the observed results, it seems that the rectangular barrier model does not fit our data. Others have used the rectangular barrier model to analyze tunneling in molecular systems and in junctions. Becka and Miller,<sup>39</sup> using data from electrochemical measurements, and Majda,<sup>60</sup> using data from J<sub>Hg–SAM//SAM–Hg</sub> junctions, used eq 11 to calculate tunneling barrier heights from measured values of the attenuation factor  $\beta$ . Their values of  $\beta = 0.8$ – $0.9 \text{ \AA}^{-1}$  yielded barrier heights of  $\sim 1.2 \text{ eV}$ ; this value is inconsistent with their observations that the values of  $\beta$  they measured changed by  $<10\%$  over a range of bias potentials of  $\sim 1 \text{ V}$ . These authors also concluded that the rectangular barrier model was not compatible with their observations. They did not propose an alternative. Only Mann and Kuhn found good agreement of their experimental data with this model.<sup>48</sup>

**(iii) Modifying the Rectangular Barrier Model To Provide a Model Compatible with Experiment.** The  $I$ – $V$  data calculated using a model of tunneling through an unstructured rectangular barrier do not fit our results or those reported by others. This disagreement is not surprising: the model is the simplest possible, and in real systems the barrier has molecular structure, is three-dimensional, and is never rectangular.<sup>95,112</sup> As a simple, adjustable fitting parameter, we introduced  $\alpha$  in the exponential terms of eq 8 to modify the energy term. This

(110) The HOMO-LUMO gap for polyethylene, measured by photoemission spectroscopy, is approximately 8 eV (Fujihara, M.; Inokuchi, H. *Chem. Phys. Lett.* **1972**, *17*, 554–557). This value suggests that the barrier height should be  $\sim 4 \text{ eV}$  for aliphatic SAMs.

correction factor has been used previously by Holm<sup>113</sup> and Simmons<sup>93</sup> to modify the rectangular barrier to examine tunneling through parabolic barriers as approximations of the effect of image potential.<sup>114</sup>

We again used a nonlinear least-squares method to fit eq 9 ( $\alpha \neq 1$ ) to an observed  $I$ - $V$  curve; here, the preexponential factor for  $C_{0=1}$  was fixed at 1, and  $\phi_0$  and  $\alpha$  were allowed to vary. This analysis yielded values of  $\phi_0 = 2.1$  V and  $\alpha = 0.62$ . The  $I$ - $V$  curve calculated from these parameters was in good agreement with the observed  $I$ - $V$  curve (Figure 9C).<sup>115</sup> A value of  $\phi_0 = 2.1$  V is compatible with a barrier composed of aliphatic thiols in the junction if the Fermi level of the electrode is nearly halfway between the HOMO and LUMO of the alkane chain<sup>110</sup> and it is similar to barrier heights (obtained by variable-temperature experiments) for tunneling through fatty acids.<sup>49</sup> Introducing these values of  $\phi_0$  and  $\alpha$  into eq 10 yielded values of  $\beta = 0.9 \text{ \AA}^{-1}$ ; this value does not change as a function of applied voltage, in agreement with the experimental data.

The physical interpretation of  $\alpha$  is open: we favor attributing the role of  $\alpha$  to the presence of a heterogeneous, nonrectangular barrier. As we have used it,  $\alpha$  provides a way of relating nonrectangular barriers to a functional form for rectangular ones. The value of  $\alpha$  does not, by itself, provide useful information about the structure of the barrier or the tunneling trajectory. A new theoretical model that incorporates molecular structure into the tunneling barrier is now under study.<sup>116</sup>

**(f) Mechanism Responsible for Current.** Electron tunneling in metal-SAM-metal junctions depends strongly on the position of the Fermi level of the metal electrodes relative to the HOMO and LUMO of the molecular bridge.<sup>97,100</sup> When the difference in energy between the Fermi level and the LUMO is large, electron transport occurs by superexchange tunneling: that is, tunneling that is mediated by interactions between donor and acceptor and unoccupied orbitals of the organic material separating them.<sup>97,109</sup> If the Fermi level approaches the energy of the molecular orbitals of the bridge, the mechanism of transport is resonant tunneling: that is, the electrons actually populate the bridge.<sup>101</sup> Phenomenologically, these two tunneling regimes differ in the dependence of the current on distance and applied potential. Superexchange<sup>92,97</sup> predicts an exponential decrease in current with distance; resonant tunneling predicts a weak distance dependence.<sup>97</sup> For superexchange, current should be linear with bias voltage at low potentials and increase exponentially; in the resonant regime, current should increase sharply, approaching Ohmic behavior.<sup>97</sup> The  $I$ - $V$  curves in Figures 2 and 3 show clearly the linear and exponential portions of the increase in current in response to the applied potential. These results are compatible with superexchange. Since values of  $\beta$  for aliphatic and aromatic thiols are independent of voltage over the range 0.1–1 V, we conclude that the mechanism of electron transport is also independent of voltage over this range,<sup>39,60</sup> and that the height of the tunneling barrier is significantly greater than 1 V.

(111) Figure included in the Supporting Information.

(112) *Tunneling Phenomena in Solids*; Burstein, E., Lundqvist, Eds.; Plenum Press: New York, 1969.

(113) Holm, R.; Kirschstein *Z. Tech. Phys.* **1935**, *11*, 488–494.

(114) The effect of the image potential on an electron in a tunneling junction is to reduce the area of the potential barrier between the electrodes by rounding off the corners and reducing the height and the width of the barrier.<sup>93,94,112</sup>

(115) The Supporting Information includes a discussion of the confidence intervals for the fitted  $I$ - $V$  curves. We find that the confidence integral is ~10% of the fitted value at each applied potential.

(116) V. Mujia and M. A. Ratner, personal communication.

## Conclusions

We have described a metal-SAM-metal junction that serves as a new experimental system for measuring rates of electron transport across a variety of thin organic films. The values of the attenuation factor  $\beta$  for polyalkyl,  $\beta = 0.8$ – $0.9$ , and polyphenyl chains,  $\beta = 0.5$ – $0.7 \text{ \AA}^{-1}$ , are similar to those found for these structures when used as molecular bridges in D-B-A systems. These results strongly suggest that both aliphatic and aromatic compounds do not show strong electronic interaction among the chains organized into SAMs.

Our studies of these junctions has revealed several characteristics. From the observations that current density decreases exponentially with the distance separating the electrodes and that it depends exponentially on the square root of the applied potential (eq 9), we conclude that the mechanism of transport is superexchange tunneling. This result is that expected based on prior work.<sup>48,61,92,93,112</sup> The system does not seem to be strongly influenced by the conditions used to prepare the SAMs or by the roughness of the solid silver film supporting the SAM. The van der Waals interface between the SAM on Hg and the SAM on Ag does not represent an insurmountable barrier to tunneling and its relative location between the electrodes does not have a significant effect on the magnitude of the current density. The absolute magnitude of the current density in these junctions is in agreement with the Hg-SAM//SAM-Hg junctions described by Majda; it is substantially higher (at the values of  $d_{\text{Ag,Hg}}$  we have examined) than the current density flowing across junctions having L-B films on Al/Al<sub>2</sub>O<sub>3</sub> that were described by Mann and Kuhn. We have fit the  $I$ - $V$  curves using a model derived for tunneling through a rectangular barrier that was modified empirically to allow for deviations from rectangularity by introducing an exponential term  $\alpha$  (eq 9). Although the magnitude of  $\alpha$  that we infer ( $\alpha \sim 0.6$ ) seems reasonable for a parabolic-shaped barrier based on estimates of this factor,<sup>93</sup> it cannot be interpreted uniquely in terms of structure in a barrier. We conclude from this fitting that, at minimum, a successful treatment of tunneling must assume a barrier more complex than an unstructured, two-dimensional, rectangular barrier.<sup>112</sup> A model that incorporates the molecular structure of the SAMs is under analysis to interpret our data both qualitatively and quantitatively.<sup>116</sup>

These junctions have advantages and disadvantages relative to other systems as the basis for correlating rates of electron transport with molecular structure. Their advantages are the following: (i) They are particularly easy to assemble and use. (ii) They support a range of organic structures. (iii) They are mechanically stable. (iv) They allow the collection of statistically significant numbers of measurements. (v) They allow (and require) measurement of currents over small but significant areas (~1 mm<sup>2</sup>, or ~10<sup>12</sup> molecules) of contact, and thus average variations in current due to boundaries between metal grains and organic domains, differences in local structure of the SAM, and small defects. (vi) They allow rates of electron transport to be measured over a wide range of values without changing instrumentation. (In this study, we measured current densities over a range of approximately 8 orders of magnitude). (vii) They allow rates of electron transport to be correlated directly with molecular structure, with at least some knowledge of the conformation of the organic molecule with respect to the surface of the electrode. (viii) The electrodes can be made of different metals (Ag, Au, Cu, Hg) and alloys. (ix) The junctions can probably be extended to systems other than thiols. The disadvantages of these junctions are the following: (i) They do not have the molecular level resolution that makes measure-

ments using STM<sup>61</sup> and break junctions<sup>55–57</sup> so informative. (ii) They will not support measurements over a broad range of temperatures. (iii) They probably cannot be developed into practically useful microelectronic components.

We propose that these junctions provide a useful new experimental tool for investigations of electron transport across organic thin films. This system should be particularly valuable for physical organic studies, that is, for screening the electrical properties of a wide range of molecular structures for their ability to support electron transport. Its principal advantage is the simplicity with which it can be assembled and used. This simplicity should allow these junctions to complement physics-based experimental methods that require difficult fabrication or complicated and expensive equipment.

## Experimental Section

**Materials.** Alkanethiols ( $\text{HS}(\text{CH}_2)_n\text{-CH}_3$  ( $n = 8, 10, 12, 14, 16$ )), thiophenol ( $\text{HS}(\text{Ph})\text{H}$ ), and benzylthiol ( $\text{HSCH}_2(\text{Ph})\text{H}$ ) were purchased from Aldrich or TCI and were used without further purification. We prepared 4-biphenylthiol ( $\text{HS}(\text{Ph})_2\text{H}$ ), 4-methylene-biphenylthiol ( $\text{HSCH}_2\text{-}(\text{Ph})_2\text{H}$ ), 4-triphenylthiol ( $\text{HS}(\text{Ph})_3\text{H}$ ), and 4-methylene-triphenylthiol ( $\text{HSCH}_2(\text{Ph})_3\text{H}$ ) according to procedures described previously.<sup>117,118,119</sup> Anhydrous ethanol (Pharmaco, 200 proof) was used to dissolve alkanethiols, thiophenol, and benzylthiol; the oligophenylene thiols were dissolved in anhydrous tetrahydrofuran (J. T. Baker). Electronic grade mercury (99.9998%) was purchased from Alpha. *Caution: Mercury is highly toxic if swallowed or if its vapors are inhaled.* Hexadecane was purchased from Aldrich.

**Fabrication. (a) SAMs.** SAMs on silver were prepared by immersing a freshly evaporated thin film of silver ( $\text{Ag}(111)$ ; 2000 Å) in a solution of the appropriate thiol (10 mM) in ethanol or THF. The SAMs were allowed to form at room temperature over 24 h. The silver film was prepared by thermal evaporation (Edwards Auto 306) of an adhesion layer of chromium (~50 Å thick) onto a 3-in. Si/SiO<sub>2</sub> wafer (Silicon Sense, test grade) followed by a layer of silver (~2000 Å thick). After the evaporation chamber was filled with nitrogen gas, the metal film was removed and immediately immersed in the solution of thiol; it was then transferred through air to the solution of thiol. The SAM-coated silver surfaces were removed from the solution of thiol, rinsed with ethanol or THF, and dried under a stream of dry nitrogen. These surfaces were then ready to be incorporated into junctions. SAMs on mercury were formed by extruding a drop of liquid mercury from a capillary (~5 μL) and exposing it to an aerated solution of thiol (10 mM) in ethanol or hexadecane for ~10 min. After the SAM formed on the drop of mercury, it was removed from the solution of thiol and rinsed with ethanol or hexadecane; the SAM-coated mercury was then used to assemble the junction.

**(b) Junctions.** The junctions were assembled as described previously:<sup>59</sup> a SAM-coated silver film was placed in a beaker and covered with a solution of hexadecane containing the thiol used to form SAM-(2) (usually hexadecanethiol) at a concentration of ~1 mM; this thiol increases the stability of the junction.<sup>59</sup> The Ag-SAM was connected electrically to an electrometer by an alligator clip in contact with the silver surface. The SAM-coated hanging mercury drop, supported by a gastight syringe (1 mL; Hamilton), was immersed in the hexadecane

solution above the Ag-SAM. A tungsten wire protruding from the Teflon tip of the syringe plunger provided an electrical connection between the mercury electrode and an electrometer. The syringe suspending the mercury drop was held by a micromanipulator, and the micromanipulator was used to bring the SAM-coated drop of mercury into contact with the surface of the SAM on Ag. The contact areas were determined by video microscopy: a video camera with a 50× objective was used to image the junction and display the image on a video monitor. The diameter of the circular area of interfacial contact between the two organic films was estimated on the video screen with calipers; this diameter was compared to the magnified diameter of the syringe tip to estimate the real diameter of contact.  $I$ - $V$  curves were measured with the electrodes attached to an electrometer (Keithley 617 programmable electrometer). The electrometer was used to apply the potential and to measure the current through the junction. The voltage ramp was applied as a staircase function with steps of 50 mV and with an interval of at least 5 s between steps. These parameters were chosen based on the estimated resistive-capacitive (RC) time constants of the junctions ( $C_{\text{junction}} \sim 10^{-10}$  F). The potential was increased in steps over the range of 0 to 1 V, or to the BDV.

We estimated the distances separating the metal surfaces in  $\text{J}_{\text{Ag-SAM}(1)/(2)\text{SAM-Hg}}$  junctions ( $d_{\text{Hg,Ag}}$ ) by adding the thickness of SAM(1) on silver and the thickness of SAM(2) on mercury. The thickness of the SAM on mercury generated from  $\text{HS}(\text{CH}_2)_{15}\text{CH}_3$  ( $\text{C}_{16}\text{-Hg}$ ; 2.34 nm) was estimated using an algorithm<sup>60</sup> that assumes the alkanethiol to be in the extended, all-trans conformation and oriented normal to the mercury surface.<sup>120</sup> To estimate the thickness of the aliphatic SAMs on silver, we used the algorithm employed for the Hg-SAMs, but multiplied it by  $\cos(12^\circ) = 0.98$  to account for a tilt of 12° from the normal for alkanethiols on silver.<sup>121</sup> The resulting thicknesses are in good agreement with measurements of the capacitances of these junctions.<sup>58</sup> Aromatic SAMs are also known to have a tilt angle of ~10° from the surface normal on silver.<sup>122,123</sup> For the aromatic SAMs on silver, we used a minimized structure (MM2; Chem 3D) to determine the distance from the sulfur atom to the terminal hydrogen atom, and added the length of the Ag-S bond (0.23 nm); we assumed that in the SAM, the thiol was oriented vertically with respect to the metal surface and added an additional 0.1 nm to account for the van der Waals radius of the terminal hydrogen atom.

**Acknowledgment.** This work was supported by the ONR, DARPA, and the NSF (ECS-9729405). R.E.H. and M.L.C. thank the National Institutes of Health for postdoctoral fellowships and R.H. thanks the Deutsche Forschungsgemeinschaft and the BASF-fellowship program for financial support.

**Supporting Information Available:** Experimental details of control experiments, plots of current-voltage data, and a detailed discussion of the statistical analysis of the data (PDF). This material is available free of charge via the Internet at <http://pubs.acs.org>.

JA004055C

(120) Deutsch, M.; Magnussen, O. M.; Ocko, B. M.; Regan, M. J.; Pershan, P. S. *Thin Films (San Diego)* **1998**, *24*, 179–203.

(121) Laihinis, P. E.; Whitesides, G. M.; Allara, D. L.; Tao, Y. T.; Parikh, A. N.; Nuzzo, R. G. *J. Am. Chem. Soc.* **1991**, *113*, 7152–67.

(122) Sabatani, E.; Cohen-Boulakia, J.; Bruening, M.; Rubinstein, I. *Langmuir* **1993**, *9*, 2974–81.

(123) Kang, J. F.; Ulman, A.; Liao, S.; Jordan, R.; Yang, G.; Liu, G. *Langmuir* **2001**, *17*, 95–106.

(117) Sabatani, E.; Cohen-Boulakia, J.; Bruening, M.; Rubinstein, I. *Langmuir* **1993**, *9*, 2974–2981.

(118) Tao, Y.-T.; Wu, C.-C.; Eu, J.-Y.; Lin, W.-L. *Langmuir* **1997**, *13*, 4018–4023.

(119) Himmel, H.-J.; Terfort, A.; Wöll, C. *J. Am. Chem. Soc.* **1998**, *120*, 12069–12074.